Second International Symposium on Marine Propulsors
smp'11, Hamburg, Germany, June 2011

Propulsion Enhancements for a Greener Environment

D. Hafermann, J. Marzi[1]

[1] Hamburg Ship Model Basin, HSVA, Hamburg, Germany

ABSTRACT

In anticipation of new regulations ruling energy efficiency on board ships and also in view of the actual development of oil prices, fuel economy is more than ever of prime importance to all commercial ship operations. Improving propulsive efficiency, particularly through the application of add-on Propulsion Improvement Devices (PIDs), appears to be an option not only for newly-designed vessels but also as retro-fit for existing ships. Assessing the potential benefits of PIDs, however, remains a crucial issue.

While the use of CFD for hullform optimisations with respect to resistance improvements represent the state-of-the-art today, more advanced numerical modelling techniques are now applied to simulate a complete numerical propulsion test and to analyse the effect of different PIDs. Using HSVA's in-house RANS code FreSCo$^+$, the effects of fins and a duct on a tanker hull and pre-swirl stator on a container vessel have been analysed after validating the code for a common test case. The potential of the devices considered has been evaluated.

Keywords

CFD, Numerical Propulsion Test, Energy Efficiency, Propulsion Improvement Devices

1 INTRODUCTION

In the past 20 years the share of waterborne transport in green house gas production has increased rapidly. This is due to the greater volume of transport and the reduction of emissions in other industrial sectors. The majority of different future transport scenarios evaluated in the IMO's MEPC – Green House Gas Study (MEPC 95 (2009)) predict a significant rise in transport volume and, along with this, a rise of fuel consumption and hence associated emissions. Despite the recent political reverse, e.g., at the Copenhagen Summit, it is evident that the world is in dire need to react and cut green house gas emissions as far as possible. To do so, two different options are available. The first valuable contributions will be to apply all kind of technologies helping to clean exhaust gas and thus reduce dangerous emissions to improve the balance achieved on an individual vessel as well as at fleet level. Energy recovery, e.g., from exhaust gases, promises significant contributions and is regarded as an important element of reducing ship-borne GHG emissions. On the other hand, recovered energy will be available to power other consumers on board a ship, but very rarely for ship propulsion. This however, in case of most freight carrying vessels, is the predominant factor determining the main engine installed on board a ship which constitutes the principal "level of consumed energy" for those vessels. Improving the energy efficiency in a way that primary resources will be saved, hence, requires an improvement of the hydrodynamic system so that less energy is required to propel the ship.

It is common knowledge that IMO expects to introduce the Energy Efficiency Design Index (EEDI) and the Energy Efficiency Operational Index (EEOI) shortly, and it can be foreseen that these indices will be applied not only to new build ships but also to existing ships. Anticipating these developments, new solutions need to be sought to substantially improve energy efficiency.

The two primary factors influencing power consumption are i) the total resistance R_T of the vessel, and ii) the propulsive efficiency η_D determined by the propeller and its arrangement behind the hull. Designing a new vessel will allow to address both aspects during the design process and find optimised solutions over a range of operating conditions. This, however, is not an option for the existing fleet. Today's economic restrictions further result in a life-time extension of ships already operating. At the same time, more ships are operating at lower speed ("slow steaming") and, hence, in slightly off-design conditions. To improve propulsive power delivery and thus fuel efficiency for existing vessels with changed operational profiles, modifications of the hull form to reduce resistance is mostly not an option. The focus, therefore, has to lie on the second factor contributing to the equation: the propulsive efficiency. Determined by the propeller and its arrangement, this part lends itself more easily to further improvements also for existing vessels. The choice here ranges from using more suitable propeller designs to modifications of the overall propeller arrangement behind the ship, which, in most cases however, will result in a costly modification of the ship's aftbody too. In addition to these measures, today a range of energy saving devices promises improvements of

overall efficiency through recovering parts of the losses of the propeller slipstream or to improve the propeller inflow. In the present paper, the RANS code FreSCo$^+$ is applied to analyse a set of energy saving or propulsion improvement devices (PID) with respect to their potential to contribute to fuel efficiency in shipping, thereby at the same time reducing exhaust gas emissions.

Whilst numerical simulations have been commonly applied during the past decade to optimise hull forms with respect to resistance, state-of-the-art methods nowadays allow to further address complete propulsion optimisations using a coupled approach. Besides giving integral values such as thrust, torque, resistance and propulsion efficiency, the advantage of numerical methods lies in a detailed insight into the local as well as overall flow phenomena. In this paper, numerical simulations of the effects of different propulsion improving devices with the RANS code FreSCo$^+$ are presented. The computational results show good agreement with experimental data. The application of the highly automated numerical propulsion test yields an encouraging outcome. The results show that FreSCo$^+$ is a valuable tool to assess the effects and, thus, the optimization of propulsion improving devices, also in respect to full scale prediction.

2 NUMERICAL METHODOLOGY

2.1 The FreSCo$^+$ code

The FreSCo$^+$ code solves the incompressible, unsteady Navier-Stokes-equations (RANS) (Schmode & Hafermann 2006, Schmode et al 2006, Hafermann 2007). The transport equations are discretized with the cell-centred finite volume method. Using a face-based approach, the method is applied to fully unstructured grids using arbitrary polyhedral cells. Therefore, the code can use grids from different grid generators, such as the fully unstructured, automatic grid generator HEXPRESS. This reduces the time needed for generating typical grids from several days down to several hours. The governing equations are solved in a segregated manner, utilising a volume-specific pressure correction scheme to satisfy the continuity equation (Ferziger & Peric 2002). To avoid an odd-even decoupling of pressure and velocity, a third-order pressure smoothing is employed along the way, which is outlined by Rhie & Chow (1983). The fully implicit algorithm is second-order accurate in space and time. The approximation of integrals is based on the mid-point rule. Diffusion terms are approximated using second-order central differences, whereas advective fluxes are approximated based on blends between high-order upwind-biased schemes (e.g., QUICK), first order upwind and second order central differences schemes. The resulting linear equation systems are solved iteratively using Krylov subspace methods. The respective solvers are provided by the PETSc library (Balay et al 2010). The code is efficiently parallelized in space using the message passing interface (MPI). To account for turbulent flows, additional transport equations are solved for turbulent quantities. Several turbulence models are implemented in the code: k-ε (Standard, RNG, and Chen), k-ω (Standard, BSL, and SST), Menter's One Equation model and the Spalart-Allmaras turbulence model.

2.2 The Numerical Propulsion Test

To perform a numerical propulsion test, the code FreSCo$^+$ is coupled with HSVA's in-house vortex lattice code QCM (Streckwall 1991) (Quasi Continuous Method) for propellers in an iterative fashion (Chao 2000, Chao 2001) as outlined in Figure 1.

At the start of the simulation, a nominal wake distribution is extracted from the converged RANS solution without the propeller effect. This distribution and an estimated turning rate are used as an input for the QCM code to compute the propeller thrust and torque. The turning rate is adjusted until the propeller thrust required to overcome the ship resistance (in propulsion mode) is obtained. The hydro-dynamic forces of the propeller are converted in form of body forces which are assigned to cells within the swept volume resulting from rotation of the propeller blades.

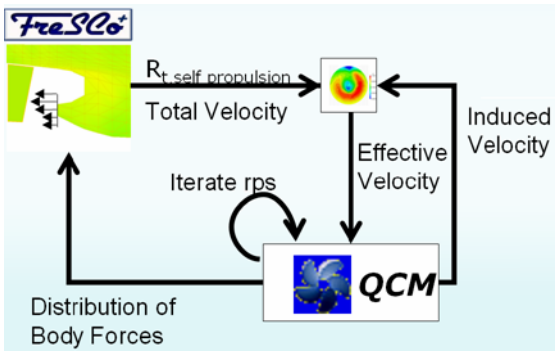

Figure 1: Numerical Propulsion Test Scheme

The resulting distribution of the body forces is used as an input to a next RANS calculation loop. The RANS computation is continued in the next iteration cycle and a new total velocity field is created. The propeller induced velocities of the last cycle, which are an output of the QCM code, are subtracted from the total velocity field. The resulting effective wake distribution is used as input in the subsequent QCM calculation. The iteration is repeated until the equilibrium between the resistance of the ship under self-propulsion condition and the propeller thrust is reached.

3 VALIDATION EXCERCISES

3.1 Open Water Computations

In order to validate the code for propulsion applications, open water computations were performed using the RANS solver FreSCo$^+$ and the vortex lattice code QCM for a range of different propeller configurations. The results were compared to model tests performed at HSVA. In Figure 2 the open water characteristics of a typical five-bladed propeller is shown. The agreement between the measurement and both the vortex lattice and the RANS computations is very good.

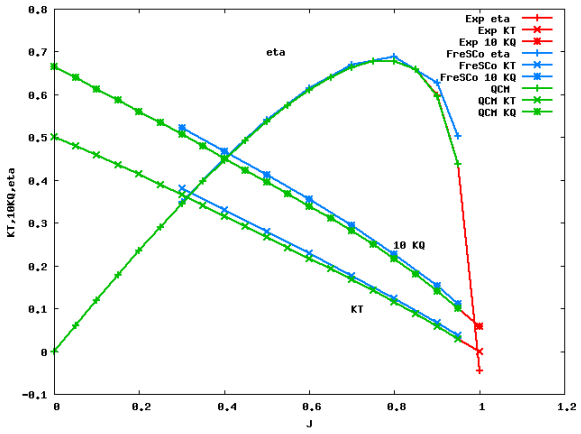

Figure 2: Open Water Characteristics for a Five-Blade Propeller.

3.2 Numerical Propulsion Tests

To validate the procedure of numerical propulsion test, the Hamburg Test Case (HTC), a modern container ship of CB =0.645, was selected. The Reynolds number is 2.9 10^6 for the model scale. Figure 3 shows the history of the computed hull resistance without and with propeller effect. New body forces are computed with the iterative method described above and used as input to the RANS code. The change of the force history due to the coupling can be clearly seen. After about 1500 RANS iterations the forces converged to a constant value. The resulting computed propeller turning rate is 8.22 rps compared to 8.32 rps in the experiment.

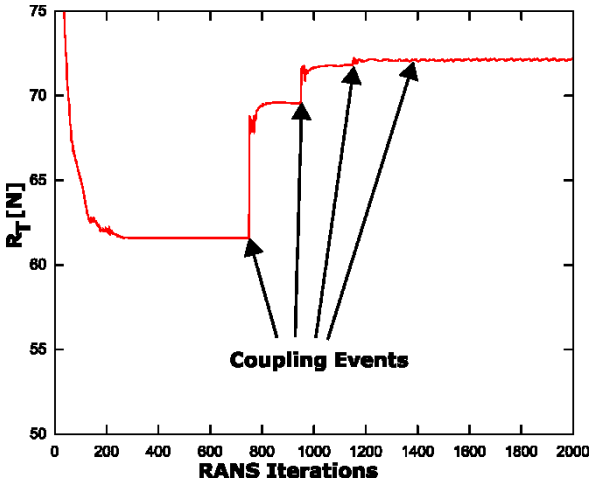

Figure 3: Hamburg Test Case: History of Hull Resistance

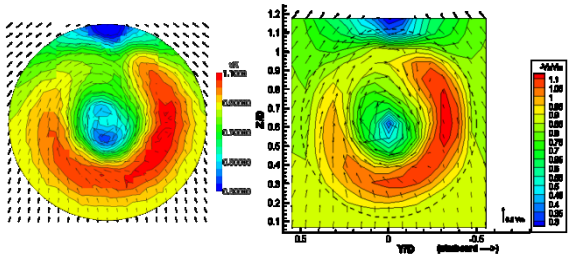

Figure 4: Hamburg Test Case: Axial Velocity Behind Propeller (Computations/Measurements)

Figure 4 shows the computed and measured velocity distributions at $(x-x_p)/D=-0.201$ behind the propeller. The agreement is good.

Figure 5 gives an impression of the free surface distribution at the transom for the flow with (above) and without (below) propulsion. The differences are very small. The comparison of the numerical propulsion test results obtained with and without free surface is given in Table 1. The differences are due to different account of the wave resistance, which is not considered in the double body flow predictions.

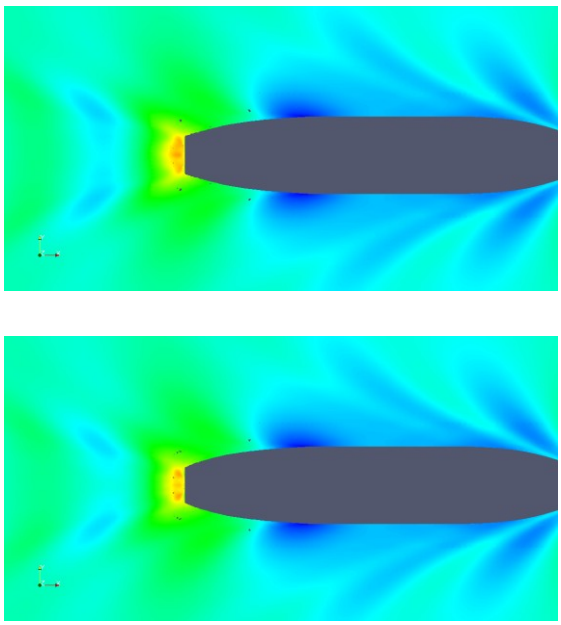

Figure 5: Hamburg Test Case: Stern Wave pattern (with Operating Propeller – top; without Propeller – bottom)

	T[N]	Q[Nm]
Experiment	56.25	2.05
Double Body	47.31	1.84
Free Surface	53.83	2.05

Table 1: Hamburg Test Case: Comparison of Double Body and Free Surface Computations.

4 Result of PID Studies

4.1 Tanker

Two different types of propulsion improvement devices have been analysed for a tanker hull: a set of foils mounted well before the propeller and a duct, all intended to equalise the wake distribution. The geometries of the tanker without and with PIDs –fins or fins and duct – are shown schematically in Figure 6. The calculations were performed for a speed corresponding to a Froude number Fn of 0.153. To facilitate the studies, double-body flow computations were considered. The wave making resistance was computed with a VOF computation for the bare hull, including the reaction type rudder, and was added to the double body results.

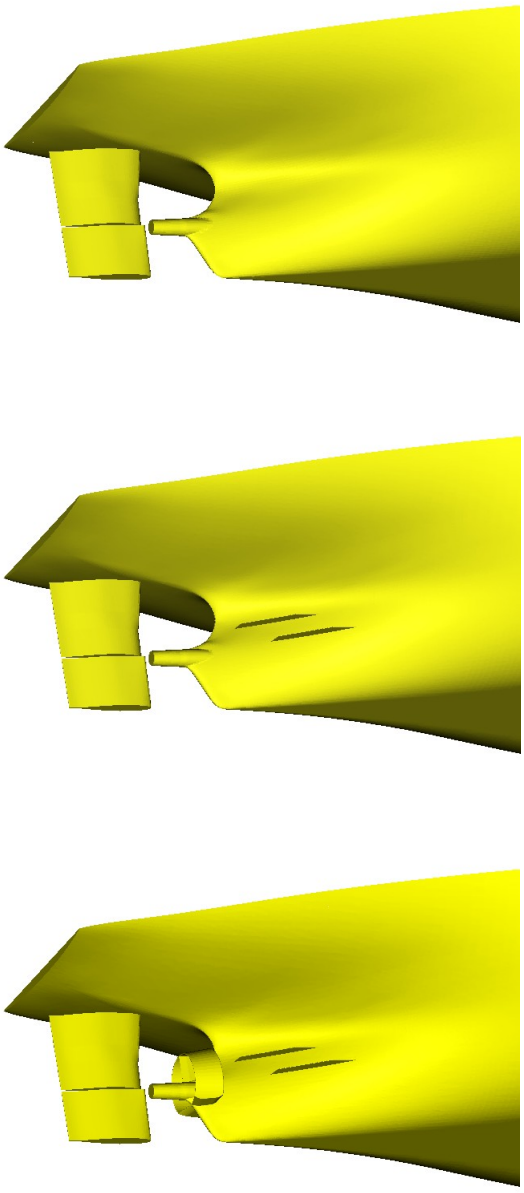

Figure 6: Tanker Hull Geometries and PIDs

All computational grids were generated using the software HEXPRESS. The grid sizes were 3.6 million cells for the bare hull with rudder, 5.8 million cells for hull, rudder and fins, and 8.1 million cells for the configuration hull with rudder and duct. The distance of the first cell at the wall was adjusted for computations with wall functions. The capability of using a fully unstructured grid allows grid refinement close to the propulsion improving devices. A hull mesh with grid details near the mentioned PIDs is shown in Figure 7. The standard k-ω turbulence model of Wilcox was applied in all computations.

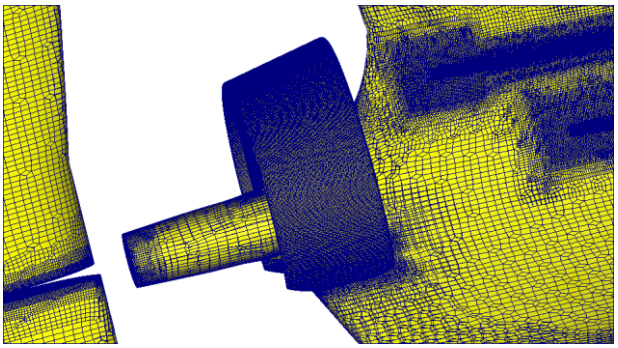

Figure 7: Tanker: Grid Detail

Figures 8 to 10 show the computed wake distributions in the propeller plane (left) compared to the experimental results (right) for the tanker. The computational results agree well with experiments for the test cases of bare hull with ruder and hull with rudder and fins. Experimental results were not available for the case of the hull with fins and duct.

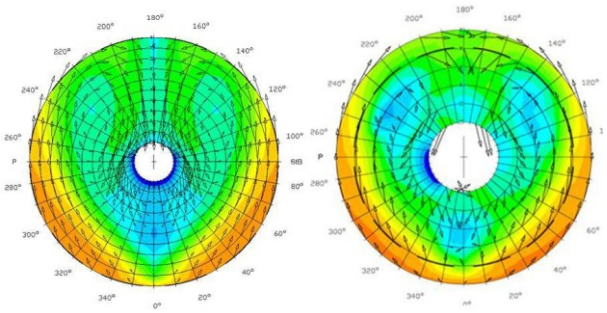

Figure 8: Tanker: Nominal Wake Distribution, Distributions in Propeller Plane for Bare Hull with Rudder (Computations/Measurements)

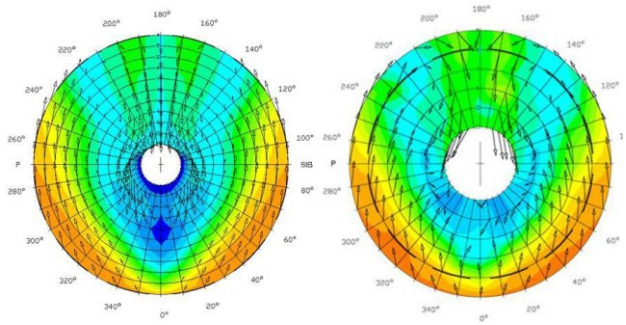

Figure 9: Tanker: Nominal Wake Distributions in Propeller Plane for Bare Hull with Rudder and Fins (Computations/Measurements)

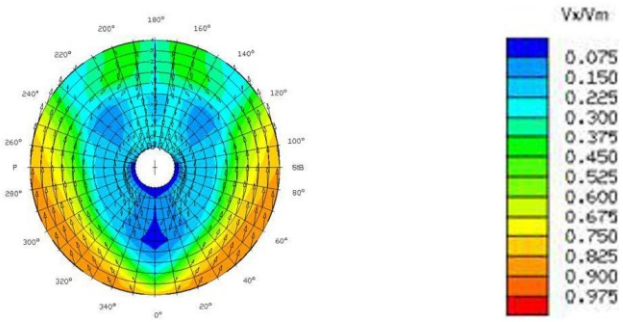

Figure 10: Tanker: Nominal Wake Distribution in Propeller Plane for Hull with Duct and Fins (Computation)

The use of the different propulsion improving devices leads to a smaller tangential component of velocity on the port side, which is a desired effect to reduce propeller slip loss. Taking the respective experimental results for the bare hull with rudder as the basis for comparison, the normalised integral quantities are shown in Table 2. The experimental values are listed above the computed results for each corresponding configuration. The experimental values for configuration without propulsion improving devices were set to 100% - all other column values are related to these values. The model tests gave the same resistance for the hull with fins case, and a reduction of the total resistance of about 2.7 percent for the configuration hull with fins and duct. The computations showed an increase of resistance for the hull with fins by 1 percent and a similar increase of resistance for the hull with fins and duct.

When performing the numerical propulsion tests, the same friction deduction force as applied for the model self-propulsion test was used to compensate the relatively higher frictional resistance of the model, so that the model propeller would be correctly loaded.

Main outputs of a propulsion test are the turning rate N, the thrust T and the torque Q of the propeller. During the model tests, an additional towing force F_D is applied to compensate for the for the model's additional surface friction (compared to the full scale ship). This force is accounted for in the computations as well.

The effective power is defined by:

$$P_E = R_T \cdot V = (R_{Tm} - F_D) \cdot V_m \cdot \lambda^{3.5} \cdot \rho / \rho_m \qquad (1)$$

The power delivered at the propeller is:

$$P_D = 2\pi \cdot n \cdot Q = 2 \cdot \pi \; n_m \cdot Q_m \cdot \cdot \lambda^{3.5} \; \rho / \rho_m \qquad (2)$$

The resulting propulsion efficiency is defined as:

$$\eta_D = P_E / P_D \qquad (3)$$

An indicator for the efficiency gain is the relation between the propulsion efficiency of the configuration with rudder and the configuration with rudder and PID. The values highlighted in the last column of Table 2 were obtained for experiments (E) and CFD computations (C) separately. The tendency of efficiency improvement shown in model test was correctly predicted by the numerical propulsion test; the computed improvement is, however, smaller compared to the experiment.

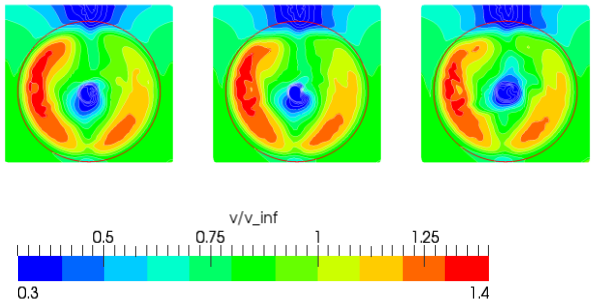

Figure 11: Tanker: Axial Total Velocity Distribution in a Plane behind Propeller (From left: No PID, with Fins, with Fins and Duct)

We know from the propulsion theory that even for optimal hull forms there are propulsion losses. For right-hand single-screw ships the propeller rotates in the same direction on the port side as the tangential component of the inflow; the so-called propeller slip loss leads to lower thrust and efficiency on the port side. As pointed out above, the tangential velocity component on the port side was reduced through the installations of fins and duct for the present tanker. Thus, a positive effect of these PIDs could be expected.

Another propulsion loss is the slipstream loss behind the propeller, in terms of the kinetic energy losses. For the present case study, the computed total velocity fields in a plane at $(x-x_p)/D=-0.20$ behind the propeller are shown in Figures 11 and 12 for the axial and the transverse component, respectively.

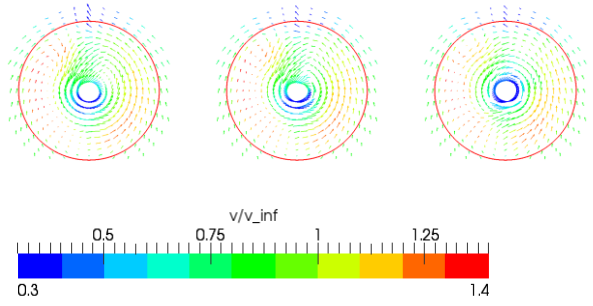

Figure 12: Tanker: Transverse Velocity Vectors in a Plane behind Propeller (From left: No PID, with Fins, with Fins and Duct).

The kinetic energy of the fluid within a cylinder volume of unit length in the propeller race (behind the propeller) may be expressed as:

$$E_{ke} = \frac{1}{2}\iint V^2 \rho dm = \frac{1}{2}\iint \left(Vx^2 + Vy^2 + Vz^2\right)\rho r d\theta dr \qquad (4)$$

where Vx, Vy and Vz are the total velocity components. To compare the different configurations, the corresponding velocity components are integrated over

the propeller circle in the plane shown in Figures 11 and 12 Figure. The integral of the total kinetic energy of the configuration hull with fins and hull with fins and duct are 0.5 and 2.2 percent lower than for the configuration with rudder, respectively. The rotational energy is reduced by 10 percent for the fins and by about 30 percent for the fins and duct configuration. Larger kinetic energy of the fluid in the propeller slip-stream is nothing different than a larger propulsion loss. From the results derived from Figures 11 and 12, it can be stated that there are differences in translational (axial) kinetic-energy loss, and that the configuration hull with duct has the least rotational energy loss. These results are in agreement with the results of numerical propulsion tests shown in Table 1.

	PID	Rtm [%]	N [%]	T [%]	Q [%]	η_D	$\eta_{D,PID}/\eta_{D,Bare}$
E	-	100	100	100	100	0.75	
C	-	100	99	101	106	0.71	
E	Fins	100	97	96	95	0.81	**1.084**
C	Fins	101	99	102	107	0.73	**1.021**
E	Fins Duct	97	95	92	91	0.82	**1.094**
C	Fins Duct	101	100	98	104	0.73	**1.022**

Table 2: Tanker: Result of the Numerical Propulsion Test.

4.2 Container Ship

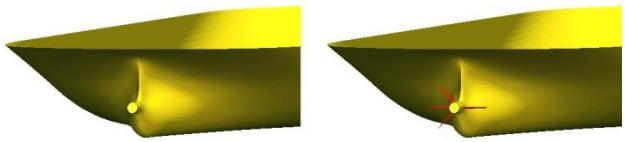

Figure 13: Container Ship: Hull Geometry and Pre-Swirl Stator

The second example compares a large container ship with and without pre-swirl stator (PSS) in front of the propeller. The hull geometry and the pre-swirl stator are shown in Figure 13. The ship and the pre-swirl stator device were designed by Daewoo Shipbuilding & Marine Engineering (DSME).Three blades are arranged on the port side and one blade is arranged on the starboard side. The Froude number at design speed was 0.21 and double-body viscous flow computations were considered; the wave making resistance was estimated based on panel method. The grid sizes were 1.7 million cells for the bare hull and 4.1 million cells for the hull with pre-swirl stator. Figure 14 shows the mesh at stern and the stator. The standard k-ω turbulence model of Wilcox was applied in all computations.

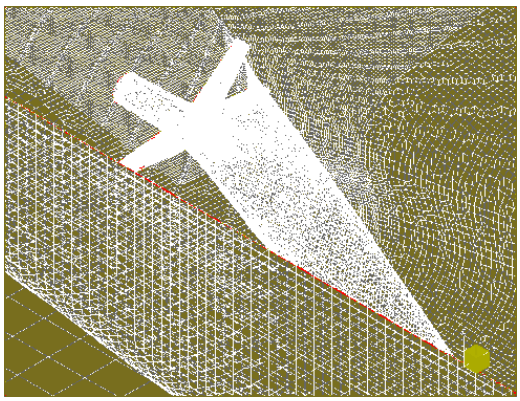

Figure 14: Container Ship: Unstructured Grid Detail at Stern and Pre-Swirl Stator

The computed and the measured nominal wake distributions in the propeller plane are shown in Figures 15 and 16, respectively. The influence of the pre-swirl stator blades can be clearly detected by the three distortions of the axial velocity distributions and the reduced tangential component on the port side. These lead to a favourable inflow to the propeller. The normalised integral quantities are shown in Table 3. The agreement between the predicted resistances and the measurements is very good.

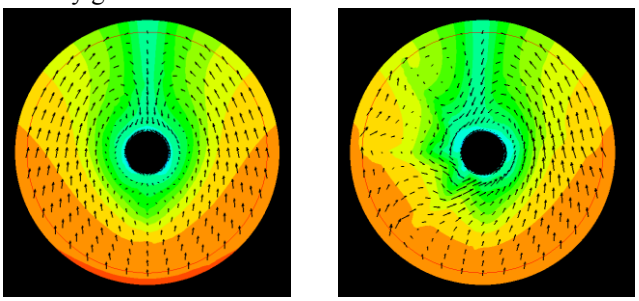

Figure 15: Container Ship: Computed Velocity Distribution in Propeller Plane (Bare Hull / with Pre-Swirl Stator).

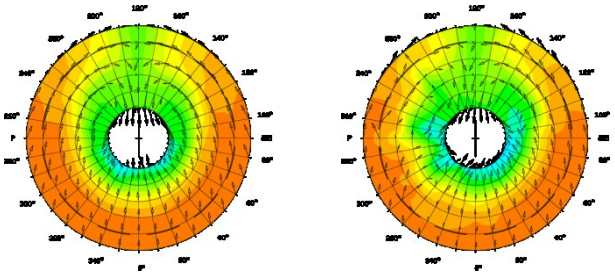

Figure 16: Container Ship: Measured Velocity Distribution in Propeller Plane (Bare Hull / with Pre-Swirl Stator).

The results of the numerical propulsion test for the container ship are given in Table 3 as normalised quantities for the experiments (E) and the computations (C). The agreement between the model tests and the computed results are very good. The efficiency gain has been predicted accurately.

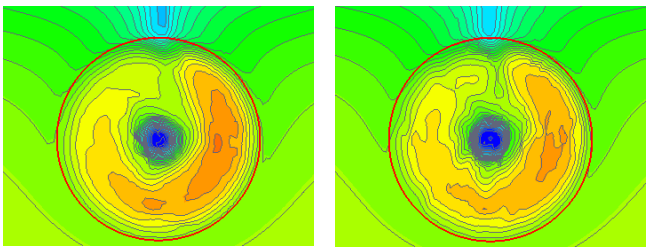

Figure 17: Container Ship: Total Axial Velocity Distribution in a Plane behind the Propeller. (Left: Bare Hull; right: with Pre-Swirl Stator)

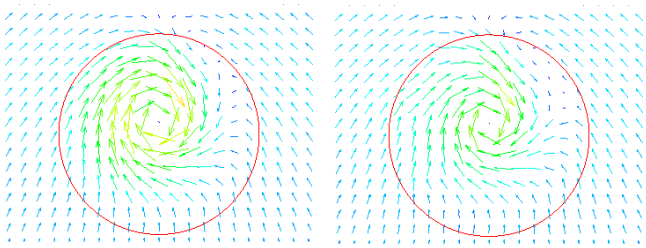

Figure 18: Container Ship: Transverse Velocity Vectors in a Plane behind Propeller. (Left: Bare Hull; right: with Pre-Swirl Stator

As mentioned above, the gain in efficiency can be explained by comparing the relative slip loss due to the tangential component of the inflow and the kinetic energy losses in the slip stream of the propeller. The distributions of the total axial and transverse velocity components in the plane at $(x-x_p)/D=-0.20$ behind the propeller plane are shown in Figures 17 and 18, respectively. For the configuration with pre-swirl stator, the translational and the rotational kinetic energy losses in propeller slip stream are about 4% less than in the case of bare hull. Thus, the pre-swirl stator improves the propulsion efficiency, as confirmed by the experiment.

	PID	Rtm [%]	N [%]	T [%]	Q [%]	η_D	$\eta_{D,PID}/\eta_{D,Bare}$
E	-	100.0	100.0	100	100.0	0.75	
C	-	99.3	99.1	100	92.8	0,80	
E	PSS	(100)	96.8	101	98.6	0.78	**1.05**
C	PSS	100.6	96.1	101	93.1	0,85	**1.06**

Table 3: Container Ship: Results of the Numerical Propulsion Test.

4.3 Potential Benefits of Propulsion Improvement Devices

The different types of PID investigated for i) the tanker hull, and ii) the container vessel indicate quite significant improvements in propulsive efficiency. With η_D increasing more than 2% (8% experiment) for the tanker hull and 5% for the container vessel significant reductions in fuel consumption can be expected. Assuming an estimated engine power of 30,000 kW and state-of-the-art fuel consumption rates, annual fuel costs for one vessel will be abt. 4.8 M€ based on current prices. Saving 5% yield cost savings of abt. 240 k€ per year, or, in ecological terms, a reduction of CO_2 emissions of about 5200 ts per year. At fleet level, these reductions are of course even more significant. If we estimate a number of 100 vessels converted in the course of 1 year, this would yield already almost half a million ton of CO_2 emission reductions annually.

Present estimates indicate that necessary investments for the installation of customised PIDs will lead to a return on investment of about 3 years which appears to be a reasonable period. It must, however, be noted that a sound analysis and customisation of the different devices is required to take full benefit of the technology.

5 CONCLUSIONS

The established numerical propulsion test using HSVA's novel RANS code FreSCo$^+$ shows encouraging results when applied to the analysis of a variety of different types of propulsion improvement devices. The computational results are in good agreement with experimental investigations and, hence, prove the method to be a viable tool for the investigation of the potential of PIDs to be used for both new build vessels as well as for retro-fit.

The application of the highly automated numerical propulsion test demonstrates that FreSCo$^+$ is a valuable tool to assess the effects and hence the optimisation of propulsion improving devices, also in respect to full scale prediction.

Anticipated savings in terms of fuel costs as well as reduced green house gas emissions for PIDs are significant and are expected to pay off investment costs over a relatively short period.

REFERENCES

Balay, S, K., Buschelman, K., Gropp, W. D., Kaushik, D., Knepley, M. G., Curfman McInnes, L. , Smith, B. F. & Zhang , H. (2010). PETSc Web page, http://www.mcs.anl.gov/petsc.

Chao, K. Y. (2000). 'Vereinfachte Methode zur Leistungsprognose unter genauer Erfassung der Wechselwirkung zwischen Schiffsrumpf". Ruder und Propeller HSVA Bericht **1637**.

Chao, K. Y. (2001). 'Numerical Propulsion Tests". Ship Technology Research (Schifftechnik) **48**(2), June.

Ferziger, J. H. & Peric, M. (2002). Computational Methods for Fluid Dynamics. 3rd ed. Springer Verlag.

Hafermann, D. (2007). 'The New RANSE Code FreSCo for Ship Application'. STG Jahrbuch **2007**.

HEXPRESS. (2010). Full Hexahedral Grid Generation, http://www.numeca.be/index.php?id=29.

MEPC 59. (2009). 'Second IMO GHG Study Prevention of Air Pollution from Ships'.

Rhie, C. M. & Chow, W. L. (1983). 'A numerical study for the turbulent flow an isolated airflow with trailing edge separation'. AIAA Journal **17**, pp. 1525.

Schmode, D. & Hafermann, D (2006). 'Comparison of Wind Tunnel Measurements and Computations with RANS Solver FreSCo'. NuTTS symposium, Varna, Bulgaria.

Schmode, D., Vorhölter, H., Rung, T. & Hafermann, D. (2006). 'RANS-Based Flow Analysis for Propellers and its Benefits'. 7th Int. Conf. On Hydrodynamics, Ischia.

Streckwall, H. (1991). 'Eine instationäre Vortex-Lattice Methode für den Schiffspropeller'. Proceedings Rostocker Schiffstechnisches Symposium, Rostock.